Z. Phys. Chem. **218** (2004) 905–914

CO Oxidation on a $Pd/Fe_3O_4(111)$ Model Catalyst

By R. Meyer, Sh. K. Shaikhutdinov*, and H.-J. Freund

Department of Chemical Physics, Fritz-Haber-Institut der Max-Planck-Gesellschaft, Faradayweg 4–6, Berlin 14195, Germany

Dedicated to Prof. Dr. Gerd Wedler on the occasion of his 75th birthday

(Received April 1, 2004; accepted April 22, 2004)

Iron Oxides / Magnetite / Palladium / CO Oxidation / Size Effect

Adsorption of CO and O_2 on Pd particles deposited on a well-ordered $Fe_3O_4(111)$ film was studied by temperature programmed desorption. Scanning tunneling microscopy was used to provide structural information. The results show that CO adsorbed on Pd particles reacts with oxygen of the oxide support and forms CO_2. The reaction occurs at the particle/oxide interface and exhibits a particle size effect such that the smaller particles produce more CO_2. Oxidation of Pd/Fe_3O_4 alters the oxide structure due to Pd catalyzed oxygen migration into the film and results in formation of an oxygen reservoir, which favors CO oxidation reaction.

1. Introduction

It is generally considered that catalysts supported on reducible oxides may exhibit different catalytic performances than those on non-reducible supports, particularly in oxidation reactions. This stems from the fact that the reducible oxide can supply oxygen atoms and be directly involved in the reaction schemes (Mars–van Krevelen mechanism) [1]. The nature of the support may also influence particle morphology and size distribution, and in some cases lead to a phenomenon referred to as a strong metal support interaction (SMSI). SMSI was originally developed as an explanation for the decreased chemisorption of CO and H_2 on metal particles and is most notably observed for Pt and Pd particles on TiO_2 [2, 3]. A well-documented manifes-

* Corresponding author. E-mail: shaikhutdinov@fhi-berlin.mpg.de

tation of SMSI is the encapsulation of metal particles by the reduced oxide support [3–12].

In order to gain a deeper understanding of these phenomena and to elucidate mechanisms of the oxidation reactions at a molecular level, well-defined model systems, including metal particles deposited on an ordered oxide film, have been developed [13–15]. In our laboratory, we have extensively studied reactivity of Pd model catalysts supported on alumina films [15–18]. The nucleation and growth of Pd has been also studied on other oxide surfaces as well, including single crystals of MgO(100) [19], α-Al_2O_3(0001) [20], ZnO(0001) [21], TiO_2(110) [22–24], and silica [25], chromia [26], magnesia [27], ceria [11] and most recently by our group on FeO(111) films [28].

In this paper, we focus our studies on Pd deposited on the Fe_3O_4(111) films and report on CO and O_2 adsorption and their interaction using temperature programmed desorption (TPD). Low energy electron diffraction (LEED) and scanning tunneling microscopy (STM) were used to provide the structural information.

2. Experimental

The experiments were performed in an UHV chamber (base pressure below 10^{-10} mbar). The chamber was equipped with STM, LEED, an Auger spectrometer (all from Omicron) and a differentially pumped quadrupole mass-spectrometer (QMS, Fisions).

The Fe_3O_4(111) films were prepared by cycles of iron deposition and oxidation [29]. In each cycle, about 3–5 ML of Fe (99.99%, Advent) were evaporated onto a Pt(111) substrate and subsequently oxidized in *ca.* 10^{-6} mbar O_2 at 900 K for 5 min. The final oxidation was carried out at 1000 K. The quality of the films was checked by LEED and STM prior to Pd deposition.

Palladium (99.99%, Goodfellow) was deposited on the oxide film at ~ 100 K with a deposition rate of *ca.* 0.5 Å min^{-1}. The pressure during metal depositions never exceeded 5×10^{-10} mbar. For each Pd coverage studied, new oxide films were grown.

Iron and palladium were deposited with commercial evaporators (Focus EFM3). During deposition, the sample was biased with a retarding potential in order to prevent metal ions from being accelerated towards the sample. Deposition rates were calibrated with a quartz microbalance. The Pd coverage is presented in the paper as a nominal thickness (in Å).

Oxygen and CO (both 99.999%, AGA Gas) were exposed to the samples with a calibrated directional gas doser. The mass spectrometer signals were corrected with ionisation gauge sensitivities 1.36 for CO_2 and 1.02 for CO.

The STM images were taken at room temperature using Pt-Ir tips at bias ~ 1.4 V and current ~ 1 nA, with the observed features independent of bias polarity.

3. Results and discussion

The $Fe_3O_4(111)$ films exhibited sharp LEED patterns. The STM images of the clean films showed flat terraces separated by steps of ~ 5 Å in height (or multiple) corresponding to the monoatomic steps. High resolution images revealed that the terraces exhibited a hexagonal lattice of protrusions with a ~ 5 Å periodicity (see also Fig. 1(b)). Based on *ab initio* calculations, the protrusions were previously assigned to the iron cations terminating the surface [29]. Accordingly, the missing protrusions were attributed to the iron vacancies. It should be however mentioned that although the $Fe_3O_4(111)$ films and single crystals were previously studied by several groups using LEED and STM [29–31], the surface structure is not well understood. In order to get more information about surface termination of the $Fe_3O_4(111)$ surface, recently we have employed combined TPD and infrared spectroscopy of CO as a probe molecule, which will be discussed in more detail in the forthcoming paper [32]. Here we only note that TPD spectra of CO adsorbed at 80 K on clean $Fe_3O_4(111)$ films show three desorption peaks centred at 105, 160 and 230 K (see also Fig. 2(a)). Consecutive CO TPD spectra were essentially identical, thus indicating that the oxide film does not suffer from reduction by CO. Small traces of CO_2 detected during CO TPD (*ca.* 5% of CO signal) simply follow the CO signal and are due to the CO reactions inside the mass spectrometer ("cracking"). Indeed, exposure of CO^{16} to the film grown with O_2^{18} did not result in any desorption signal of $CO^{16}O^{18}$ (46 amu), only $CO^{16}O^{16}$ (44 amu) was detected.

Oxygen was found to molecularly desorb from the clean films in a single peak at ~ 250 K (not shown here). Therefore, the desorption temperatures of CO and O_2 from the $Fe_3O_4(111)$ surface (~ 230 and ~ 250 K, respectively) are far below than ~ 480 K and ~ 800 K observed on the Pd surfaces (for example, see Refs. [33, 34]).

Palladium deposition results in formation of hemispherical particles, which are randomly distributed on the substrate as shown in Fig. 1(a). No preferential decoration of step edges is observed by STM. Interestingly, vacancies defects and their agglomerates are still observed on the bare support between the particles as marked by the arrows in Fig. 1(b). This finding indicates that either Pd nucleates homogeneously, including the vacancy defects as well, or the interaction of Pd with the oxide is relatively weak as Pd atoms may escape the defect sites and stick to the growing particle at 300 K (STM measurement temperature).

As mentioned above, CO desorption for Pd surfaces extends out to 480 K. Therefore, we conducted CO TPD experiments to 550–600 K. Fig. 1(c) shows that Pd particles strongly sinter upon heating: the particles become larger, and their number decreases.

Three consecutively measured CO TPD spectra of $Pd/Fe_3O_4(111)$ preannealed to 600 K and dosed with 1 L of CO at 100 K are shown on Fig. 2. It

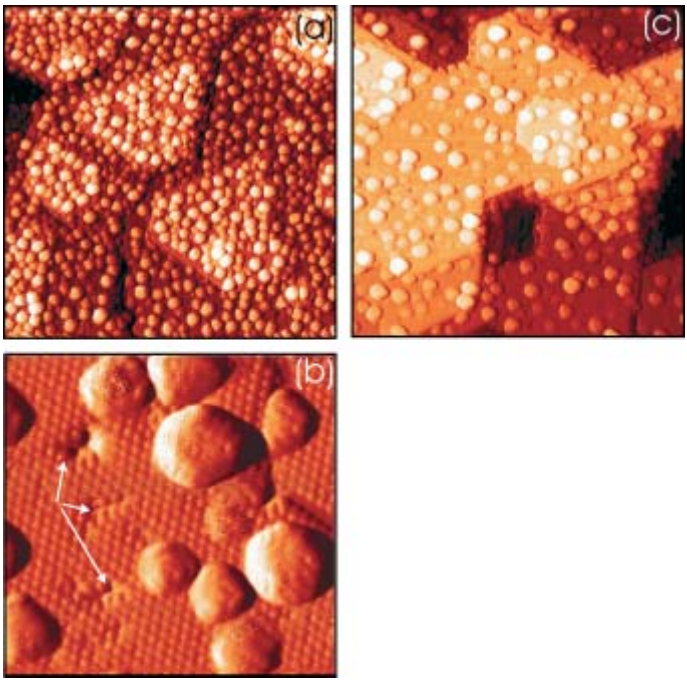

Fig. 1. STM images of Pd particles formed on $Fe_3O_4(111)$ at 100 K and warmed to 300 K (a), and then annealed to 600 K (c). High resolution image of surface (a) is shown in (b). The arrows indicate vacancy defects observed on iron oxide support. Size: $100 \times 100\,nm^2$ (a,c) and $15 \times 15\,nm^2$ (b).

is clear that the signals at temperatures below 250 K overlap with those of the bare support, which can be subtracted with a corresponding weight factor.

Meanwhile, the signal above 250 K definitely originates from the Pd particles and is very similar to those observed for Pd particles, deposited on alumina, [15, 18] and Pd single crystal surfaces [33, 34].

At low temperature, the CO_2 traces follow those of CO similar to that found for clean $Fe_3O_4(111)$ and can be readily assigned to CO cracking inside the mass spectrometer. However, the CO_2 peak at ~ 490 K originates from the reaction of CO with the Pd/Fe_3O_4 surface.

In principle, one may suggest different reaction mechanisms of CO_2 formation. For example, CO_2 is formed by the reaction of CO with hydroxyl groups:

$$CO + OH \rightarrow CO_2 + \tfrac{1}{2}H_2\,. \qquad (1)$$

However, neither Pd particles nor magnetite films possess OH groups.

Another mechanism includes CO decomposition:

$$2CO \rightarrow C + CO_2\,. \qquad (2)$$

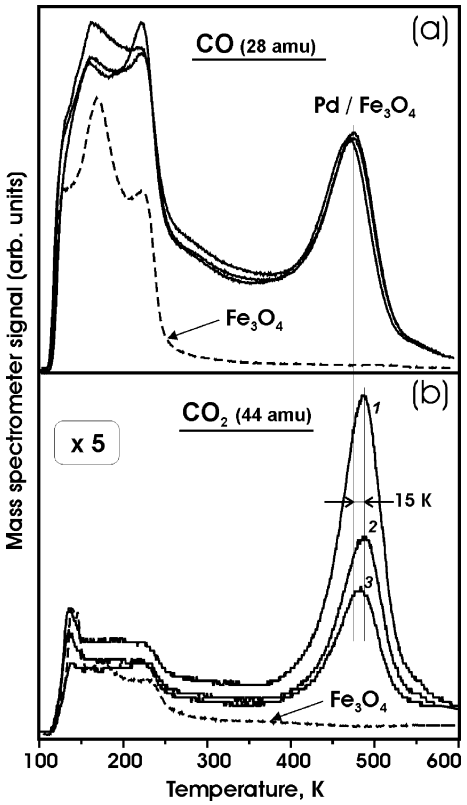

Fig. 2. CO TPD spectra for 1 L of CO adsorbed at 100 K on 0.7 Å $Pd/Fe_3O_4(111)$. Data for clean support are also shown. Formation of CO_2 on Pd particles at $\sim$ 480 K is clearly seen, which decreases with increasing number of TPD cycles (1,2,3). Note the $\sim$ 15 K difference between CO and CO_2 desorption peaks.

However, carbon residues would block CO adsorption sites and result in remarkable changes in the next CO TPD [35]. In contrast, Fig. 2 shows that intensity of CO signal does not change with increasing number of TPD runs. In addition, carbon deposition was never detected on CO exposed Pd particles deposited on alumina support by photo-electron spectroscopy [15]. Therefore, we can rule out both reactions (1) and (2) as responsible for CO_2 formation.

Bearing in mind that Fe_3O_4 is reducible oxide, we suggest that CO reacts with lattice oxygen of iron oxide to form CO_2,

$$CO + O_{ox} \rightarrow CO_2 \tag{3}$$

which desorbs immediately upon formation as CO_2 adsorbs on Pd more weakly than CO [36]. Interestingly, the reaction limited CO_2 desorbs at a temperature

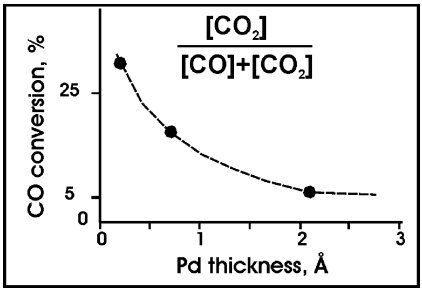

Fig. 3. CO conversion calculated by integral TPD signals of CO and CO_2 at 400–600 K, shown in Fig. 2, as a function of Pd nominal thickness.

by ~ 15 K higher than CO (see Fig. 2). This implies that CO activation is the rate-limiting step of reaction and that CO either reacts with oxygen or desorbs intact if there is no oxygen available.

We note that CO_2 produced by CO adsorption on oxygen precovered Pd surfaces exhibits a desorption maximum at ~ 400 K [18, 34], that is significantly below 490 K observed in Fig. 2. This result points to a lack of oxygen spillover from oxide to Pd, and that CO_2 is formed by reaction of CO, adsorbed on the metal particle, with oxygen present on the oxide support.

Previously, CO oxidation on Pd deposited on iron oxide film (presumably Fe_2O_3) has been studied by Kalinkin *et al.* [37], which suggested that the reaction (3) occurs at the metal/oxide interface. Therefore, the reaction should exhibit a particle size effect. Indeed, Fig. 3 shows CO conversion, calculated by TPD signal areas at 400–600 K as a function of Pd coverage. The conversion strongly increases for the smallest Pd particles. The small CO_2 signal observed for the largest particles studied is primarily due to CO reaction inside the QMS. The majority of CO molecules adsorbed on large particles desorb intact, while CO reacts and forms CO_2 on the small particles. This result can be readily explained by the increasing perimeter to surface area ratio as particle size decreases.

Since oxygen reacted with CO cannot be recovered under UHV conditions, oxygen on the support around the particles is depleted. As a result, the amount of CO_2 formed gradually decreases with increasing number of TPD runs as seen in Fig. 2. In order to re-oxidize the support, the samples were exposed to 10^{-6} mbar of O_2 at 500 K for 45 min. The structure was then analyzed by a spot-profile analysis (SPA) LEED and STM.

Fig. 4(a) shows LEED pattern of the sample containing 0.25 Å of Pd deposited at 100 K and annealed to 600 K. The pattern exhibits all spots characteristic for the $Fe_3O_4(111)$ surface [29]. After stepwise oxidation for 1, 10 and 30 min at 500 K, no new spots appeared, however, the intensity of the spots gradually attenuates, as shown in Fig. 4(b). (Note that such attenuation is not found for annealing in UHV). This means that the oxide surface becomes

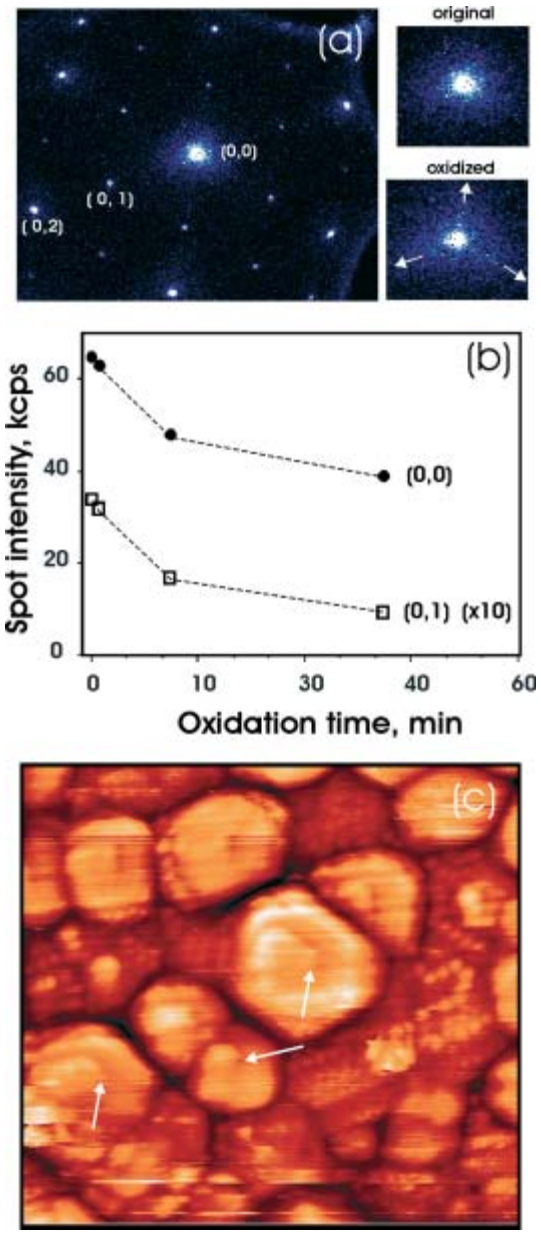

Fig. 4. (a) LEED pattern of 0.2 Å $Pd/Fe_3O_4(111)$. (b) The intensity of two selected diffraction spots as a function of oxidation time in 10^{-6} mbar of O_2 at 500 K. The (0/0) spot is zoomed for both the pristine and oxidized surfaces. (c) Typical STM image (size $15 \times 15\ nm^2$) of the oxidized sample showing that ordering is partially lost between the particles, exhibiting screw dislocations marked by the arrows (compare with Fig. 1b).

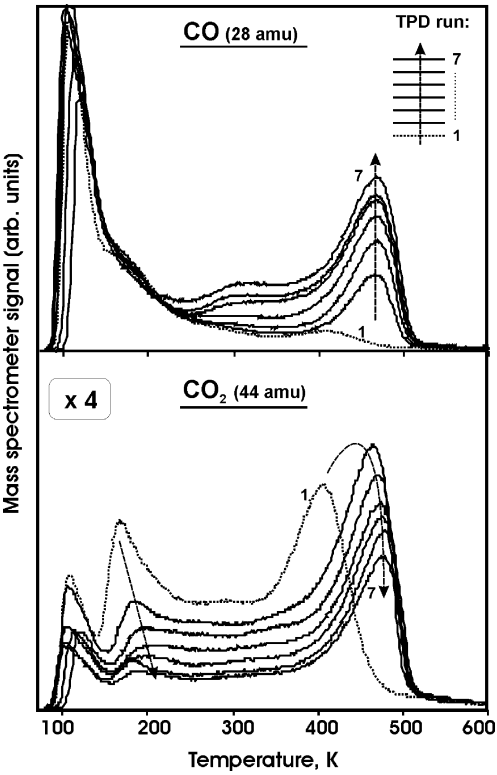

Fig. 5. CO TPD spectra for 1 L of CO adsorbed at 80 K on $Pd/Fe_3O_4(111)$ pre-oxidized at 500 K. CO and CO_2 responses are shown at increasing number of TPD cycle.

more disordered after oxidative treatment. Interestingly, the circular shape of the (0,0) spot alters such that three distinct shoulders develop along the main crystallographic directions as zoomed out in Fig. 4.

Morphological changes are also observed by STM as shown in Fig. 4(c). Firstly, the atomic scale ordering of the oxide surface, previously seen between the particles in Fig. 1(b), is partially lost, that is consistent with the LEED observations. Secondly, many particles exhibit screw dislocations, although the particle size is not changed significantly.

CO TPD spectra for the re-oxidized sample are shown in Fig. 5. During the first TPD run, two CO_2 peaks at $\sim$ 170 K and $\sim$ 400 K are observed, while CO desorption is strongly suppressed. (Again, the CO_2 signal at 100–150 K is due to CO cracking in QMS.) The peak at 400 K has previously been observed on O_2 pre-exposed Pd surfaces and is therefore assigned to the CO oxidation reaction on Pd [18, 34]. However, the second CO TPD spectrum does not show any feature at 400 K. Instead, we observe both CO and CO_2 peaks at $\sim$ 480 K, which are similar to those on pristine system (see Fig. 2). At increasing num-

ber of TPD runs, the amounts of CO gradually increase, while the CO_2 signal decreases.

The results clearly demonstrate that CO reacts with the reservoir of oxygen present in the oxide support until it gets depleted in repeated cycles of CO exposure and heating. Obviously, the oxygen atoms are produced by Pd particles, which readily dissociate molecular oxygen. These atoms may then diffuse into the oxide film and make the film less ordered as revealed by LEED. However, according to the LEED results, no new iron oxide phases are formed at these conditions. Therefore, we conclude that oxygen atoms occupy interstitial sites in the near-surface region of Fe_3O_4 resulting in the presence of accessible oxygen which can react with CO.

Turning back to the Fig. 2, showing that the amount of CO_2 produced on pristine Pd/Fe_3O_4 samples decreases with subsequent CO adsorption in a same manner as in Fig. 5 for pre-oxidized samples, one can also suggest that the CO_2 produced results from reaction of CO with readily available oxygen in the lattice whose presence stems from small deviations from stoichiometry in the Fe_3O_4 film.

In order to see how atomic oxygen interacts with the support, we have performed isotopic experiments with the iron oxide film grown with O_2^{18}. The CO^{16} TPD spectra of the $Pd/Fe_3O_4^{18}$ sample pre-treated with O_2^{16} revealed formation of $CO^{16}O^{16}$ and not of $CO^{16}O^{18}$. Therefore, it seems unlikely that significant scrambling occurs between lattice oxygen and oxygen atoms produced by Pd.

The origin of the CO_2 peak at ~ 170 K seen in Fig. 5 is unclear. We can only speculate that atomic oxygen spills from Pd to the oxide surface around the particle and sits on the $Fe_3O_4(111)$ surface. Then CO adsorbed on the oxide may react with such presumably weakly bound oxygen and produce CO_2. However, further experiments remain to be done to prove this hypothesis.

4. Conclusions

The combined TPD, LEED and STM study of Pd particles deposited on $Fe_3O_4(111)$ showed that CO reacts with oxygen of the oxide support and forms CO_2. The reaction occurs at the particle/oxide interface and exhibits a particle size effect such that the smaller particles produce more CO_2. Oxidation of Pd/Fe_3O_4 in 10^{-6} mbar at 500 K alters the oxide structure due to Pd catalyzed oxygen migration into the film and results in formation of an oxygen reservoir, which readily reacts with adsorbed CO producing CO_2.

Acknowledgement

This work was supported by TMR project “Reactivity of clean and modified oxide surfaces” (TMR Marseille) and German-Malaysian project COMBICAT.

References

1. P. Mars and D. W. van Krevelen, Chem. Eng. Sci. Spec. Suppl. **3** (1954) 41.
2. S. J. Tauster and S. C. Fung, J. Catal. **55** (1978) 29.
3. G. L. Haller and D. E. Resasco, Adv. Catal. **36** (1989) 173.
4. R. T. K. Baker, E. B. Prestridge, and R. L. Garten, J. Catal. **59** (1979) 293.
5. O. Dulub, W. Hebenstreit, and U. Diebold, Phys. Rev. Lett. **84** (2000) 3646.
6. T. Madey, F. Pesty, and H. P. Steinruck, Surf. Sci. **339** (1995) 83.
7. M. Bowker, P. Stone, R. Bennett, and N. Perkins, Surf. Sci. **497** (2002) 155.
8. R. A. Bennett, C. L. Pang, N. Perkins, R. D. Smith, P. Morrall, R. I. Kvon, and M. Bowker, J. Phys. Chem. B **106** (2002) 4688.
9. T. Suzuki and R. Souda, Surf. Sci. **448** (2000) 33.
10. J. Evans, B. E. Hayden, and G. Lu, Surf. Sci. **360** (1996) 61.
11. D. R. Mullins and K. Z. Zhang, Surf. Sci. **513** (2002) 163.
12. R. A. Bennett, P. Stone, and M. Bowker, Catal. Lett. **59** (1999) 994.
13. D. W. Goodman, J. Phys. Chem. **100** (1996) 13 090.
14. C. T. Campbell, Surf. Sci. Rep. **27** (1997) 1.
15. M. Bäumer and H.-J. Freund, Prog. Surf. Sci. **61** (1999) 127.
16. I. Meusel, J. Hoffmann, J. Hartmann, M. Heemeier, M. Bäumer, J. Libuda, and H.-J. Freund, Catal. Lett. **71** (2001) 5.
17. Sh. K. Shaikhutdinov, M. Heemeier, M. Bäumer, T. Lear, D. Lennon, R. J. Oldman, S. D. Jackson, and H.-J. Freund, J. Catal. **200** (2001) 330.
18. Sh. K. Shaikhutdinov, M. Heemeier, I. Meusel *et al.*, Surf. Sci. **501** (2002) 270.
19. C. R. Henry, C. Chapon, C. Duriez, and S. Giorgio, Surf. Sci. **253** (1991) 177.
20. C. L. Pang, H. Raza, S. A. Haycock, and G. Thornton, Surf. Sci. Lett. **460** (2000) L510.
21. H. Jacobs, W. Mokwa, D. Kohl, and G. Heiland, Surf. Sci. **160** (1985) 217.
22. C. Xu, X. Lai, G. W. Zajac, and D. W. Goodman, Phys. Rev. B **56** (1997) 13 464.
23. P. Stone, R. A. Bennett, S. Poulston, and M. Bowker, Surf. Sci. **433** (1999) 501.
24. M. J. J. Jak, C. Konstapel, A. Van Kreuningen, J. Verhoeven, and J. W. M. Frenken, Surf. Sci. **457** (2000) 295.
25. J. B. Giorgi, T. Schroeder, M. Baumer, and H.-J. Freund, Surf. Sci. Lett. **498** (2002) L71.
26. K. Wolter, H. Kuhlenbeck, and H.-J. Freund, J. Phys. Chem. B **106** (2002) 6723.
27. C. Xu, W. S. Oh, G. Liu, D. Y. Kim, and D. W. Goodman, J. Vac. Sci. Technol. A **15** (1997) 1261.
28. R. Meyer, M. Bäumer, Sh. K. Shaikhutdinov, and H.-J. Freund, Surf. Sci. Lett. **546** (2003) L813.
29. Sh. K. Shaikhutdinov, M. Ritter, X.-G. Wang, H. Over, and W. Weiss, Phys. Rev. B **60** (1999) 11 062.
30. A. R. Lennie, N. G. Condon, F. M. Leibsle *et al.*, Phys. Rev. B **53** (1996) 10 244.
31. J. Ahdjoudj, C. Martinsky, C. Minot, M. van Hove, and G. Somorjai, Surf. Sci. **443** (1999) 133.
32. C. Lemire, R. Meyer, V. Henrich, Sh. K. Shaikhutdinov, and H.-J. Freund, submitted to Surf. Sci.
33. X. Guo and J. T. Yates, J. Chem. Phys. **90** (1989) 6761.
34. G. Zheng and E. I. Altman, J. Phys. Chem. B **106** (2002) 1048.
35. Sh. K. Shaikhutdinov, M. Frank, M. Bäumer, R. J. Oldman, S. D. Jackson, J. Hemminger, and H.-J. Freund, Catal. Lett. **80** (2002) 115.
36. C. L. Kao, A. Carlsson, and R. J. Madix, Surf. Sci. **497** (2002) 356.
37. A. V. Kalinkin, V. I. Savchenko, and A. V. Pashis, Catal. Lett. **59** (1999) 115.